Modelling, simulation and measurement of fast transients in transformer windings with consideration of frequency-dependent losses

M. Popov, L. van der Sluis, R.P.P. Smeets, J. Lopez-Roldan and V.V. Terzija

Abstract: For the specification of winding insulation of transformers, it is important to know the electrical stresses to which the winding can be exposed during fast transient oscillations. These oscillations occur during switching operations performed by circuit breakers, or when gas-insulated substations (GIS) are used. Therefore one of the priorities is to use a high-frequency transformer model capable to simulating fast transient oscillations in the windings. The model presented requires only information about the geometry of the winding and the core, as well the electrical and magnetic parameters for the used materials. In the transformer model, the frequency-dependent core and copper losses are included. Numerical computations are performed with and without the core losses being taken into account. Two types of measurement are taken to verify the validity of the model. First, the voltage transients are measured and computed by the application of a step impulse with a rise time of 50 ns. Then, the transformer is switched by a vacuum circuit breaker, and the multiple reignitions, which contain oscillations with a wide frequency range, are analysed. The results verify that the model is suitable to simulate the voltage distribution in transformer windings over a wide frequency range.

1 Introduction

Experience shows that very fast transient overvoltages (VFTOs) are not only dangerous because of their amplitude, but also because of their rate of rise. When transformer or motor insulation is frequently exposed to fast transients such as switching surges, it deteriorates and finally can fail. The fact [1, 2] is that overvoltages with a lower amplitude and higher rate of rise can be as dangerous as overvoltages with higher amplitude. Transformers are normally protected by surge arresters. However, these devices limit only the amplitude of the overvoltages. In practice [2, 3], zinc-oxide arresters with R-C snubbers are found to be an appropriate protection for medium voltage circuits. Because of the high price of these devices compared with the price of distribution transformers, the utilities want to know how probable and how dangerous is the occurrence of fast transients. The study of very fast transients is also important for the design of the transformer insulation.

The model applied for the study of fast transients depends also on the type of winding. Traditionally, we can distinguish two types of models the first one is based on the coupled inductances and capacitances [4], and the other is based on transmission line theory [5, 6]. The advantage of the first type is that it can be easily implemented in simulation software, whereas the second model, which is purely mathematical, takes into account the frequency-dependent losses, but is not very easy to implement in a simulation software environment.

So far, it has been shown that the transmission line theory can be successfully applied to evaluate voltage distributions along the windings of electrical machines and transformers [5–8]. Most of the time, it is considered that, for high frequencies, the flux does not penetrate the core, and the iron core losses can be neglected accordingly. However, in [9], by measurement of transformer impedance frequency characteristics for a short-circuited transformer and a transformer under no load, it was demonstrated that the iron core does have significant influence up to approximately 100 kHz. In [10], it was reported that, even up to 1 MHz, the iron core losses influence the frequency transients.

The present paper deals with the problem of evaluation of fast transient voltages in distribution transformer windings. Therefore a refined transformer model is presented, based on transmission line theory.

The analysis was carried out for a 15 kVA single-phase test transformer with layer-type windings. The transformer has special measuring points at the 200th and 400th turns, which are accessible outside the transformer tank. The results of the voltage transients computed at the end of the first and the second layers were compared with laboratory measurements. Two types of computation were performed to give insight into how the losses influence the distribution of fast transients. The first case takes into account only copper losses, whereas, in the second case, voltage transients are computed by the frequency-dependent core losses being taken into account. In both cases, the proximity effects are

doi:10.1049/iet-epa:20060124

Paper first received 24th March and in final revised form 13th June 2006

M. Popov and L. van der Sluis are with the Faculty of Electrical Engineering, Delft University of Technology, Mekelweg 4, 2628 CD Delft, The Netherlands

R.P.P. Smeets is with the KEMA T&D Testing, Utrechtseweg 310, 6812 AR Arnhem and the Faculty of Electrical Engineering, Eindhoven University of Technology, Eindhoven, The Netherlands

J. Lopez-Roldan is with the Pauwels Trafo Belgium N.V., Antwerpseweg 167, Mechelen B-2800, Belgium

V.V. Terzija is with the School of Electrical & Electronic Engineering, The University of Manchester, Manchester M601QD, UK

E-mail: M.Popov@EWI.TUDelft.NL

taken into account. This is verified by comparison of the measured and computed admittance frequency characteristic of the transformers. Finally, in a separate experimental set-up, the transformer is switched by a vacuum circuit breaker (VCB), and the voltage transients are measured at the same measuring points. It is found that the present model is able to simulate voltage distributions along the winding for a longer period of time. Within the observed time, voltage oscillations have a broad frequency range, from a few tens of kilohertz up to a few megahertz.

2 The transformer model

The origin of multi transmission line modelling is described through the theory of natural modes [11]. When a network of N coupled lines exists, and when $\boldsymbol{Z}$ and $\boldsymbol{Y}$ are the impedance and admittance matrices, which are the self and mutual impedances and admittances between the lines, then

$$\begin{aligned} \frac{d^2\boldsymbol{V}}{dx^2} &= -\boldsymbol{Z}\boldsymbol{Y}\boldsymbol{V} \\ \frac{d^2\boldsymbol{I}}{dx^2} &= -\boldsymbol{Y}\boldsymbol{Z}\boldsymbol{I} \end{aligned} \tag{1}$$

where $\boldsymbol{V}$ and $\boldsymbol{I}$ are incident voltage and current vectors of the line. Note that $\boldsymbol{Z} \neq \boldsymbol{Y}^{-1}$. If we apply modal analysis, the system can be represented by the following two-port network:

$$\begin{bmatrix} \boldsymbol{I}_S \\ \boldsymbol{I}_R \end{bmatrix} = \begin{bmatrix} A & -B \\ -B & A \end{bmatrix} \begin{bmatrix} \boldsymbol{V}_S \\ \boldsymbol{V}_R \end{bmatrix} \tag{2}$$

where

$$\begin{aligned} A &= \boldsymbol{Y}_0 \boldsymbol{S} \boldsymbol{\gamma} \coth(\boldsymbol{\gamma} l) \boldsymbol{S}^{-1} \\ B &= \boldsymbol{Y}_0 \boldsymbol{S} \boldsymbol{\gamma} \operatorname{cos\,ech}(\boldsymbol{\gamma} l) \boldsymbol{S}^{-1} \end{aligned} \tag{3}$$

In (2) and (3), $\boldsymbol{I}_S, \boldsymbol{I}_R$ are current vectors at the sending and receiving ends of the line; and $\boldsymbol{V}_S, \boldsymbol{V}_R$ are voltage vectors at sending and receiving ends of the line. $\boldsymbol{Y}_0 = \boldsymbol{Z}^{-1}$ is the characteristic admittance matrix; $\boldsymbol{S}, \gamma^2$ – are the eigen vectors and values of matrix $\boldsymbol{Z}$, $\boldsymbol{Y}$; and l is the length of the line.

The modelling of distribution transformers and motors can be performed on a turn-to-turn or on a group-of-turns basis. Transformers are normally constructed with many turns, and therefore the above theory can be applied for a group of turns so that the storage of a large number of elements in the computer memory can be avoided. One way is by observation of some number of turns and representation of the rest of the transformer by a terminating admittance [5, 6]. Another way is the application of hybrid modelling [10]. This means that the total number of turns is split into number of groups, so that the number of a group of turns is far less than the number of turns in the transformer. The grouping should be done in such a way that the group of turns retains the information on the voltages and currents at the beginning and at the end of the observed group. If these parameters have the same value as they have on a turn-to-turn basis, then we can conclude that hybrid modelling is equivalent to modelling on a turn-to-turn basis.

For the observed case, the transformer winding is formed by layers, and therefore the easiest way to model the transformer is on a layer-to-layer basis. When the voltages in each layer are known, the procedure can be applied for each layer, and the voltages in the turns can be determined. The disadvantage of the terminal admittance model is that it is very difficult to provide the terminal admittance over a wide frequency range. Also, when a group of turns are terminated by the terminal admittance that represents the rest of the windings, the computed results are very sensitive to the variation of this admittance.

Figure 1 shows the representation of the windings by transmission lines.

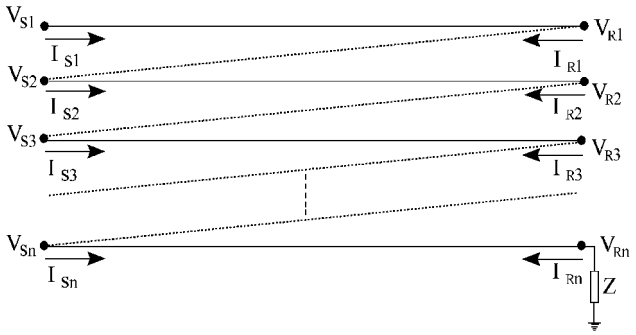

Fig. 1 *Windings or turns represented by transmission lines*

In the present case, the high-voltage winding is grounded, at the end. Therefore, convergence is produced during the computation process if the line is terminated by impedance $Z = 1 \times 10^{-9}$. Application of (2) to Fig. 1 results in the following equation:

$$\begin{bmatrix} \boldsymbol{I}_{S1} \\ \boldsymbol{I}_{S2} \\ \vdots \\ \boldsymbol{I}_{Sn} \\ \boldsymbol{I}_{R1} \\ \boldsymbol{I}_{R2} \\ \vdots \\ \boldsymbol{I}_{Rn} \end{bmatrix} = \begin{bmatrix} A' & -B' \\ -B' & A' \end{bmatrix} \begin{bmatrix} \boldsymbol{V}_{S1} \\ \boldsymbol{V}_{S2} \\ \vdots \\ \boldsymbol{V}_{Sn} \\ \boldsymbol{V}_{R1} \\ \boldsymbol{V}_{R2} \\ \vdots \\ \boldsymbol{V}_{Rn} \end{bmatrix} \tag{4}$$

In (4), A' and B' are square matrices of nth order calculated by (3). The following equations hold for Fig. 1:

$$\begin{aligned} \boldsymbol{I}_{R1} &= -\boldsymbol{I}_{S2}, \boldsymbol{I}_{R2} = -\boldsymbol{I}_{S3}, \ldots, -\boldsymbol{I}_{Rn} = \frac{\boldsymbol{V}_{Rn}}{Z} \\ \boldsymbol{V}_{R1} &= \boldsymbol{V}_{S2}, \boldsymbol{V}_{R2} = \boldsymbol{V}_{S3}, \ldots, \boldsymbol{V}_{Rn-1} = \boldsymbol{V}_{Sn} \end{aligned} \tag{5}$$

Given these equations and some matrix operations, (4) can be expressed as

$$\begin{bmatrix} \boldsymbol{I}_{S1} \\ \boldsymbol{0} \end{bmatrix} = [\boldsymbol{F}] \begin{bmatrix} \boldsymbol{V}_{Si} \\ \boldsymbol{V}_{Rn} \end{bmatrix} \tag{6}$$

In (6), $i = 1, 2, 3, \ldots, n$, and $\boldsymbol{0}$ is a zero vector of order $n \times 1$.

When we observe the model on a layer-to-layer basis, then $V_{Rn} = 0$ and, hence, (6) can be rewritten as

$$[\boldsymbol{V}_{Si}] = [\boldsymbol{H}_{i-1} \quad \boldsymbol{H}_{\chi}] \begin{bmatrix} \boldsymbol{V}_{S1} \\ \boldsymbol{0} \end{bmatrix} \tag{7}$$

where subscript $i = 2, 3, \ldots, n$, and $\boldsymbol{H}_{i-1}$ is a vector of order $(n-1) \times 1$. $\boldsymbol{H}_{i-1}$ represents the transfer function, the elements of which can be calculated from the elements of the $\boldsymbol{F}$ matrix as

$$\boldsymbol{H}_{i-1} = \frac{\boldsymbol{F}_{i,1}^{-1}}{\boldsymbol{F}_{1,1}^{-1}} \tag{8}$$

The other submatrix $\boldsymbol{H}_{\chi}$ does not have any physical meaning, because a zero vector always multiplies it.

The voltages at the end of each layer can be calculated when the voltage at the input is known and the corresponding transfer functions are calculated. The time-domain

solution results from the inverse Fourier transform

$$V_{Si}(t) = \frac{1}{2\pi}\int_{-W}^{W} \frac{\sin(\pi\omega/W)}{\pi\omega/W} V_{Si}(b+j\omega)e^{(b+j\omega)t}d\omega \quad (9)$$

for $i = 2, 3, \ldots, n$, and the $V_{Si}\ (b+j\omega) = H_{i-1}(b+j\omega)\cdot V_{S1}(b+j\omega)$.

If we divide the real and imaginary parts of the integral function, and if we apply the property of evenness of the real part and oddness of the imaginary part with respect to ω, the following expression can be used [11]:

$$V_{Si}(t) = \frac{2e^{bt}}{\pi}\int_{0}^{W} \frac{\sin(\pi\omega/W)}{\pi\omega/W} real\{V_{Si}(b+j\omega)\}\cos(\omega t)d\omega \quad (10)$$

In (10), the interval $[0, W]$, the smoothing constant b and the step frequency length $d\omega$ must be chosen properly for an accurate time-domain response to be obtained. The modified transformation requires the input function $V_{S1}(t)$ to be filtered by an $\exp(-bt)$ window function. To compute the voltages in separate turns, the same procedure can be applied.

3 Test transformer and determination of the transformer parameters

The propagation of fast surges in transformers depends on the geometrical design of the windings and the physical parameters of the insulation, such as dielectric permittivity and magnetic permeability. The electrical and magnetic properties of the windings and core must also be taken into account. High-voltage transformers are normally designed with interleaved, concentric or layer windings. Transmission line theory has so far been implemented for all types of winding, with the exception of the layer-type windings. Distribution transformers are mostly designed with layer-type windings, where layers are concentrically wrapped around the core. Another possibility is that windings are designed in a pancake form. In both cases, the transmission line theory is applicable.

The studied transformer is a single-phase 15 kVA, 6.6/0.07 kV/kV transformer, which was specially built for the investigation of transients' propagation. The transformer is equipped with special measuring points in the middle and at the end of the first layer of the transformer high-voltage side and also at the end of the second layer. All measuring points can be reached from the outside of the transformer, and measurements can be performed directly at the layers.

Figure 2 shows the winding design of the studied transformer.

The transformer is modelled on the layer-to-layer basis. As there are 15 layers, the capacitance and, consequently, the inductance matrix are of order 15×15. The capacitances are calculated by the assumption that the layers form cylindrical capacitors. As the distance between the layers is small, the assumption that the layers form plate capacitors is also correct. Therefore the capacitance matrix $\boldsymbol{C}$ is formed in the following way:

- $C_{i,i}$ is the capacitance of the layer i to ground and the sum of all other capacitances connected to the layer i
- $C_{i,j}$ is the capacitance between layers i and j taken with the negative sign $(i = j)$.

The investigation so far [12] has shown that the capacitances hardly change with the frequency. The capacitances to ground in the observed case are actually capacitances between the layers and the core. Because of the small surface of the layers, these capacitances are very low, and

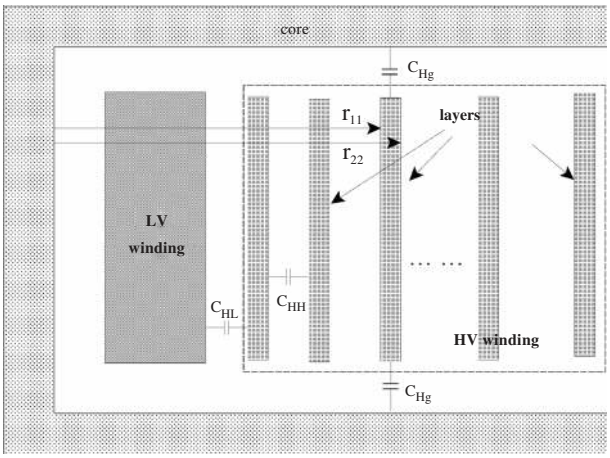

Fig. 2 *Description of layers in layer-type transformer winding*
r_{11}, r_{22} = inner and outer layer radius, C_{HH} = capacitance between neighbouring layers, C_{Hg} = capacitance between layer and core, C_{HL} = HV-LV capacitance

their value is around 1 pF. It is also found that the static voltage distribution is strongly affected by the ground capacitances. However, capacitances with values of less than 100 pF have little influence, and, for these values, the static voltage distribution can be considered as linear.

Inductances and resistances are frequency dependent. For very fast transients, especially for the first few microseconds, it is a common practice to ignore the core and eddy current losses. The inductance matrix can simply be calculated by inversion of the capacitance matrix to provide the desired speed of way propagation that depends on the dielectric and magnetic properties of the windings. Therefore the inductance matrix $\boldsymbol{L}$ is evaluated as

$$\boldsymbol{L} = \frac{\boldsymbol{C}^{-1}}{v_s^2} \quad (11)$$

where the velocity of the wave propagation v_s is calculated by

$$v_s = \frac{c}{\sqrt{\varepsilon_r}} \quad (12)$$

In (12), c is the speed of light in a vacuum, and ε_r is the relative dielectric permittivity of the transformer insulation. The oil contributes to lower equivalent relative dielectric permittivity. This implies lower values of the capacitances and inductances. Hence, dielectric and proximity losses are lower. The losses were calculated from the inductance matrix $\boldsymbol{L}$ and the capacitance matrix $\boldsymbol{C}$ [4, 5]. The impedance and admittance matrices $\boldsymbol{Z}$ and $\boldsymbol{Y}$ are then

$$\boldsymbol{Z} = \left(j\omega + \sqrt{\frac{2\omega}{\sigma\mu_0 d^2}}\right)\boldsymbol{L}$$
$$\boldsymbol{Y} = (j\omega + \omega\tan\delta)\boldsymbol{C} \quad (13)$$

In (13), the second term in the first equation corresponds to the Joule losses because of the skin effect in the copper conductor and the proximity effect. The second term in the second equation represents the dielectric losses. In (13), d is the distance between layers, σ is the conductor conductivity, and $\tan\delta$ is the loss tangent of the insulation.

In this way, the impedance matrix takes into account the frequency-dependent copper losses and the proximity effects. More generaly, the frequency-dependent core losses should be taken into account, which are important when transient oscillations with different frequencies exist. In

[13, 14], based on the analytical solution of Maxwell equations, explicit formulas for the self- and mutual impedances of coils with an arbitrary number of turns have been derived. The application of these formulas is given in Appendix.

Through this approach, it is possible to compute the $\boldsymbol{Z}$ matrix that takes into account the frequency-dependent core and copper losses. For the case studied, the order of the $\boldsymbol{Z}$ matrix is equal to the number of transformer layers. The tested transformer contains 15 layers with 200 turns per layer.

Figure 3 shows the computed mutual inductance between the first and other coils of the studied transformer. It can be seen that, for a fixed magnetic permeability μ_z and a mean magnetic path λ, and for frequencies up to 1 MHz, the mutual inductances change slightly. In this case, the mutual resistances also change little; for frequencies beyond 5 MHz, they change by around 8%.

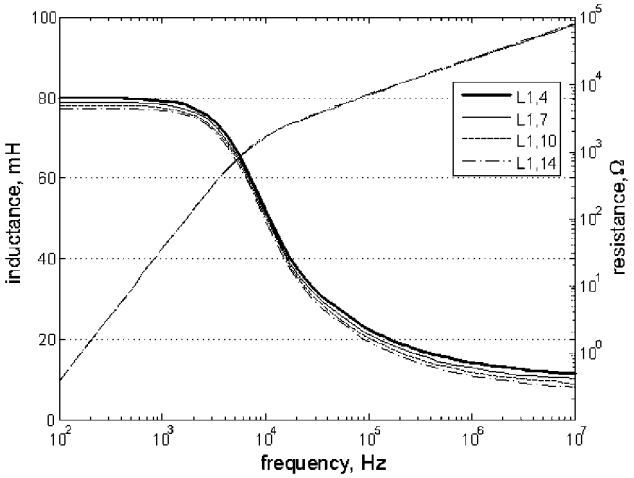

Fig. 3 *Mutual inductance and resistance between first and other coils of the studied transformer*

The value of μ_z used in the above computation is 1400 H m^{-1} and the value of the mean magnetic path of the transformer is 2 m. These two parameters are the most influential on the mutual inductance and on the proximity effects. The increase in μ_z results in an increase in the inductances and the resistances of the $\boldsymbol{Z}$ matrix, whereas a lower value of the λ contributes to lower values of $\boldsymbol{Z}$ matrix elements accordingly. By doing this, we can now apply the calculated $\boldsymbol{Z}$ and $\boldsymbol{Y}$ for each frequency in (2). By determining the element F_{11} in (6), we can find the terminal admittance of the input winding.

In Fig. 4, the measured and computed admittance characteristics are shown. The inverse Fourier transform is performed by numerical calculation of (10), with application of a step frequency $d\omega = 2500$ rad s^{-1}. Hence, the difference in the characteristics for low frequencies is notable.

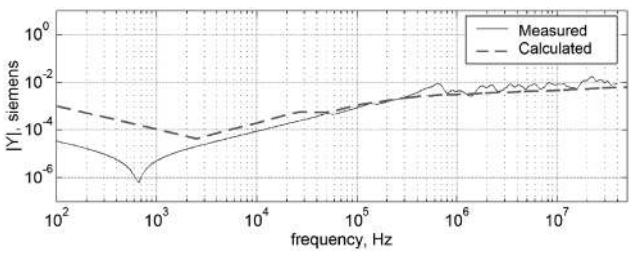

Fig. 4 *Measured and calculated terminal admittance characteristics*

Figure 4 shows that, for the transformer studied, only one resonance frequency is found below 1 kHz, which is not a subject of interest.

4 Results and validation

The measurements of fast transients for the particular measuring points are taken in the following way. A pulse generator connected to the high-voltage transformer terminal provides maximum 500 V voltage with a very short rate of rise. The full voltage is achieved within 50 ns. The transformer has special measuring points so that, apart from the terminal voltage, measurements can be taken at the end of the first layer and at the end of the second layer. In Fig. 5, the measurements and the simulations of the voltage oscillations with and without losses are presented.

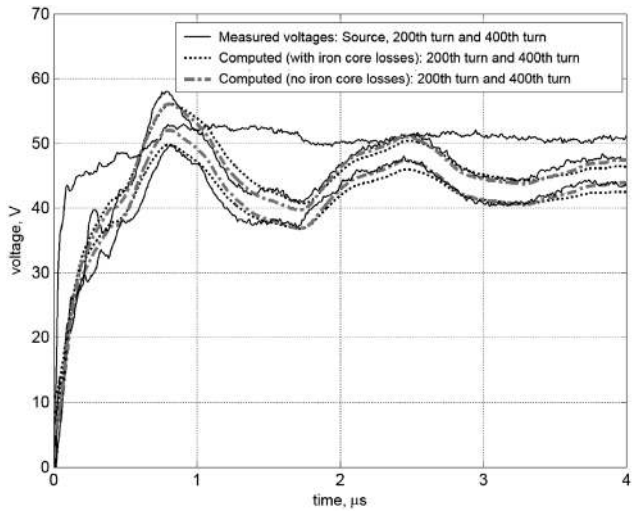

Fig. 5 *Measured and computed voltage oscillations with and without the taking into account of frequency-dependent losses*

The results, which do not take into account the frequency-dependent core losses, are produced by use of the impedance matrix defined by (13). At the first local maximum, around 1 μs, the model with the core losses shows better matching with the measured results. As it was not possible to measure the voltages at each layer, and based on the validation of the model with the presented measurements, the computed voltages in the rest of the layers are compared with those computed by the taking into account of the frequency-dependent losses.

In Fig. 6, computed voltage oscillations at specific layers are presented. For the first microsecond, the rate of rise of the voltages in both cases is almost similar. Between 1 μs and 3 μs, both lines show good agreement of the oscillation frequency and amplitude. Beyond 3 μs, the difference becomes greater. The 400th turn, the 600th turn and the other turns are affected by the losses more than the 200th turn. The layers are concentric, and the radius of the first layer is smaller than the radius of the other layers. Consequently, the inductances of the outer layers are greater than the inductances of the inner layers, which, according to (13), will contribute to higher losses. Therefore, when the input excitation to the transformer is a complex surge with oscillations with different frequencies, and the surges are observed over a longer period of time, for instance hundreds of microseconds, it is desirable to use a high-frequency transformer model that takes into account the frequency dependency of its parameters [12, 15]. In

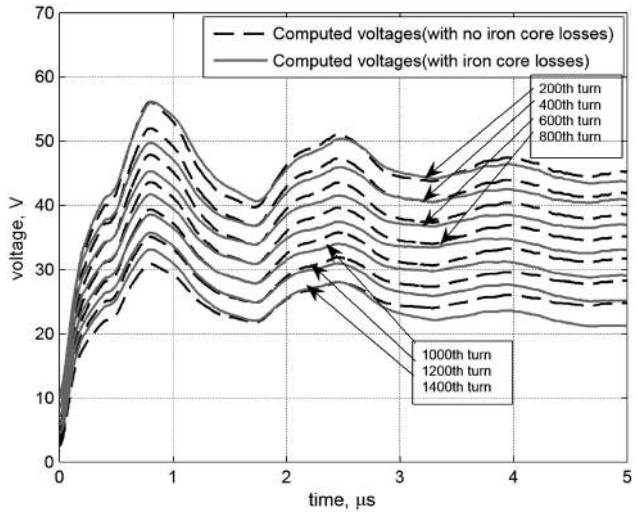

Fig. 6 *Computed voltage oscillations with and without consideration of frequency-dependent losses at specific points*

general, the frequency-dependent copper and core losses should be included.

To show the validity of the transformer model for a wide frequency range, measurements were taken of the multiple reignition overvoltages at the transformer high-voltage terminal, at the 200th and the 400th turn during switching of the transformer with a VCB. The experimental test set-up is shown in Fig. 7. The capacitor applied at the source side keeps the voltage stable after switching. The voltage at the source side is measured by a voltage transformer. An inductive load is used to provoke reignitions. The transformer is switched under a source voltage of 5 kV. The voltages are recorded at the measuring points simultaneously.

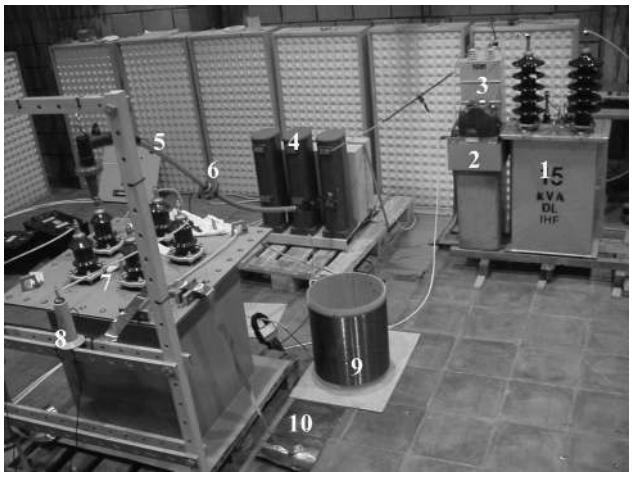

Fig. 7 *Experimental set-up*
1 = Step-up transformer, 2 = AC voltage transformer, 3 = Shunt capacitor, 4 = VCB, 5 = Cable, 6 = HF current probe, 7 = Test transformer, 8 = HF voltage probe, 9 = Inductive load, 10 = HF earthing

Figure 8 shows the measured voltage at the terminal of the transformer. This voltage is used as an input voltage that is needed to determine the other line-end coil voltages. The calculated terminal voltage is produced by using the inverse Fourier transform of the measured voltage, which is also a test that the inversion is correctly performed. Because of the different time scale of the recorded measurements, the parameters W, b and $d\omega$ in (10) must be readjusted. For this purpose, the following values are used: $W = 5 \times 10^7\,\mathrm{rad\,s^{-1}}$, $b = 500$, and the integration step $d\omega = 250\,\mathrm{rad\,s^{-1}}$.

Figures 9 and 10 represent the measured and computed voltages at the 200th turn and the 400th turn, respectively.

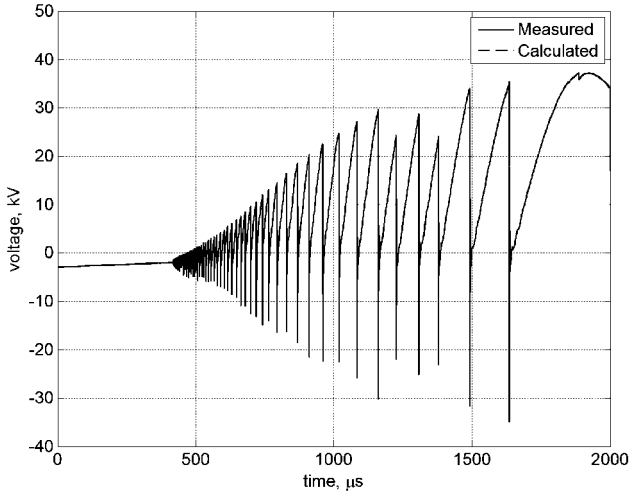

Fig. 8 *Measured and computed voltage at transformer terminal according to experimental set-up from Fig. 7*

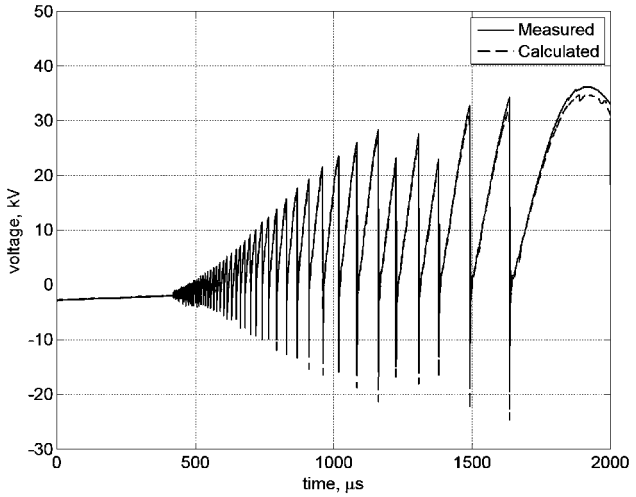

Fig. 9 *Measured and computed voltage at 200th turn according to experimental set-up from Fig. 7*

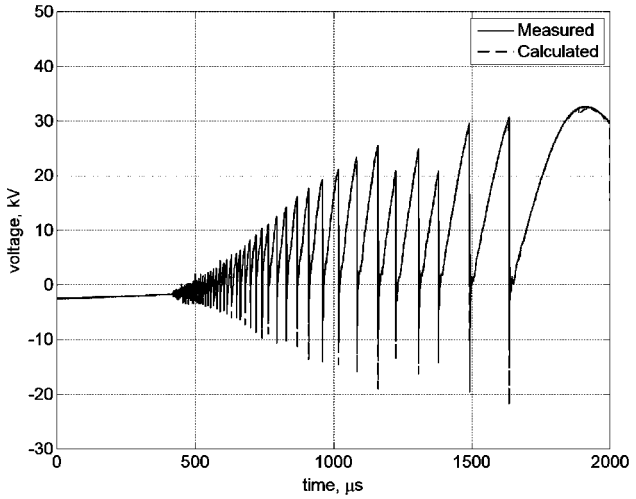

Fig. 10 *Measured and computed voltage at 400th turn according to experimental set-up from Fig. 7*

Figure 11*a* shows the enlarged values of the measured and calculated voltage of the 200th turn for reignitions between 600 μs and 700 μs. There is good matching between the calculated and measured voltage values of two adjacent reignitions. Within this region, the voltage oscillates with frequency 10 kHz and 100 kHz.

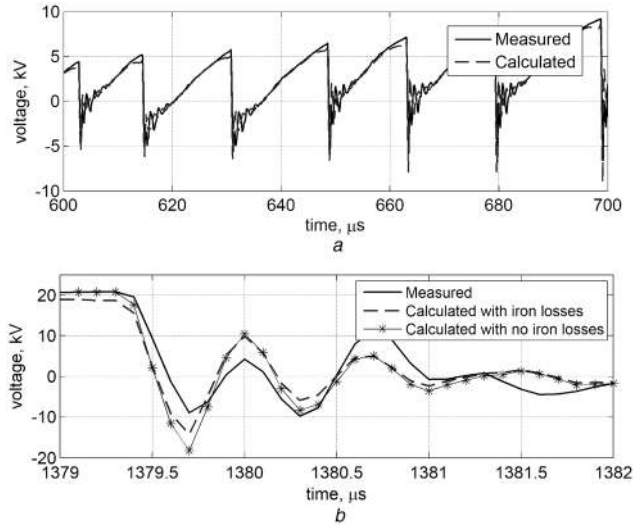

Fig. 11 *Enlarged reignitions*
a Between 600 μs and 700 μs, from Fig. 9
b Between 1379 μs and 1382 μs, from Fig. 10

Figure 11*b* shows the voltage oscillation between 1379 μs and 1382 μs from the time scale shown in Fig. 10. We observe only one reignition that occurs within 3 μs of this region. In the same Figure, the variation of the voltage is shown for the case where the iron core losses are ignored.

For very fast transient oscillations, such as those shown in Fig. 11*b*, the results can be improved by observation of a shorter time interval, for example an interval where only one reignition occurs. This allows us to apply a wider frequency range *W*. Despite the good matching of the voltages in the lower-frequency region, in the high-frequency region, the voltage oscillates with approximately the same frequency, and its amplitude is a bit higher than that of the measured voltage. This implies that the frequency-dependent copper and core losses are very important for accurate determination of very fast transients.

5 Conclusions

A computer model based on the transmission line approach and taking into account the complete iron core losses and the proximity effect between the layers has been presented. Careful attention has been paid to the more accurate representation of the transformer losses and inductances depending on frequency. The total impedance, which takes into account the influence of the winding and the iron core, is calculated at any frequency and updated in the model. This modelling of transformer winding on a layer-to-layer basis introduces the results in applicability at high frequencies and for longer time intervals. The results are verified by experimental measurements. A comparison is made with the results produced when the impedance matrix is calculated from the capacitance matrix and the speed of wave propagation. Such a representation is useful when we need to investigate the propagation of very fast transient oscillations only.

The validity of the model is verified by measurements of fast transients produced during switching of the transformer with a VCB. The method introduced here offers a possibility to predict the voltage distribution along the transformer winding when the transformer is excited by fast transient surges, which can be measured at the transformer terminal.

More work is needed for the analysis of the voltage distribution along the windings in a three-phase transformer. The model should take into account the mutual inductances and capacitances between the phase windings. It should be able to analyse the voltages due to virtual current chopping (chopping of the current in a circuit breaker pole that has not yet cleared the current, provoked by reignition of the current in another pole that attempts to clear the current) in the VCB.

6 Acknowledgment

This work was supported by the Dutch Scientific Foundation NWO/STW under Grant Veni, Det.6526.

7 References

1 Pretorius, R.E., and Eriksson, A.J.: 'Field studies of switching surge generators in high-voltage vacuum contactor controlled motors – results of extensive practical investigations'. IEE Publication 210, 1982, pp. 59–65
2 Pretorius, R.E.: 'Optimal surge suppression on high-voltage vacuum contactor controlled motor'. IEE Publication 210, 1982, pp. 65–70
3 Lopez-Roldan, J., de Herdt, H., Sels, T., van Dommelen, D., Popov, M., van der Sluis, L., and Declercq, J.: 'Analysis, simulation and testing of transformer insulation failures related to switching transients overvoltages'. CIGRE, Paris, 2002, paper 12-116
4 Shibuya, Y., and Fujita, S.: 'High-frequency model of transformer winding', *Electr. Eng. Jpn*, 2004, **146**, (3), pp. 8–15
5 Cornick, K.J., Fillat, B., Kieny, C., and Müller, W.: 'Distribution of very fast transient overvoltages in transformer windings'. CIGRE, Paris , 1992, paper 12-204
6 Guardado, J.L., and Cornick, K.J.: 'A Computer model for calculating steep-fronted surge distribution in machine windings', *IEEE Trans. Energy Convers.*, 1989, **4**, (1), pp. 95–101
7 Adjaye, R.E., and Cornick, K.J.: 'Distribution of switching surges in the line-end coils of cable connected motors', *IEE Proc.-Electr. Power Appl.*, 1979, **2**, (1), pp. 11–21
8 McLaren, P.G., and Oraee, H.: 'Multiconductor transmission-line model for the line-end coil of large AC machines', *IEE Proc. B*, 1985, **132**, (3), pp. 149–156
9 Soysal, A.O.: 'A Method for wide frequency range modelling of power transformers and rotating machines', *IEEE Trans. Power Deliv.*, 1993, **8**, (4), pp. 1802–1810
10 Shibuya, Y., Fujita, S., and Hosokawa, N.: 'Analysis of very fast transient overvoltages in transformer windings', *IEE Proc.-Gener. Transm. Distrib.*, 1997, **144**, (5), pp. 461–468
11 Bickford Pt, J.P., Mullineux, N., and Reed, J.R.: 'Computation of power system transients' (IEE, Peter Peregrinus Ltd., 1976), ISBN 0901223859
12 Guardado, J.L., and Cornick, K.J.: 'Calculation of machine winding electrical parameters at high-frequencies for switching transients studies', *IEEE Trans. Energy Convers.*, 1996, **11**, (1), pp. 33–40
13 Wilcox, D.J., Conlon, M., and Hurley, W.G.: 'Calculation of self and mutual impedances for coils on ferromagnetic cores', *IEE Proc. A*, 1988, **135**, (7), pp. 470–476
14 Wilcox, D.J., Hurley, W.G., and Conlon, M.: 'Calculation of self and mutual impedances between sections of transformer coils', *IEE Proc. C*, 1989, **136**, (5), pp. 308–314
15 Guardado, J.L., Flores, J.A., Venegas, V., and Naredo, J.L.: 'A machine winding model for switching transients studies using network synthesis', *IEEE Trans. Energy Convers.*, 2005, **20**, (2), pp. 322–328

8 Appendix

In Fig. 12, two coils with different dimensions are shown, wound around a magnetic core. The impedance in the frequency domain is

$$Z_{km} = j\omega L_{km} + Z_{1,km} + Z_{2,km} \tag{14}$$

In (14), L_{km} is the mutual inductance between the observed coils when no core exists, $Z_{1,km}$ is the mutual impedance because of the flux confined to the core, and $Z_{2,km}$ is the mutual impedance between the coils produced by the leakage flux when the core is involved. The first

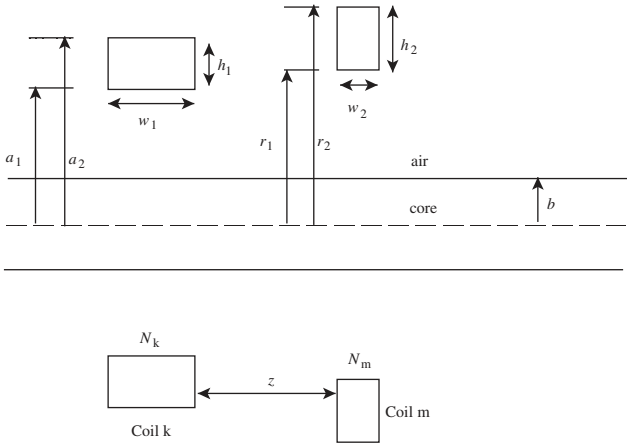

Fig. 12 *Coils of rectangular cross-section*

term in (14) is

$$L_{km} = \mu_0 N_k N_m \sqrt{ra}\frac{2}{k}\left[\left(1-\frac{k^2}{2}\right)K(k) - E(k)\right] \tag{15}$$

where $K(k)$ and $E(k)$ are elliptic integrals of the first and second kind, respectively, and k is given by

$$k = \sqrt{\frac{4ar}{z^2 + (a+r)^2}} \tag{16}$$

The other terms are

$$Z_{1,km} = j\omega N_k N_m \frac{\pi b^2}{\lambda}\left\{\frac{2\mu_z I_1(mb)}{mbI_0(mb)} - \mu_1\right\} \tag{17}$$

$$\begin{aligned} Z_{2,km} = {} & \frac{2N_k N_m}{h_1 h_2 w_1 w_2}\int_0^{\infty}\int_{-\frac{w_2}{2}}^{\frac{w_2}{2}}\int_{-\frac{w_1}{2}}^{\frac{w_1}{2}}\int_{r_1}^{r_2}\int_{a_1}^{a_2} \\ & \times\left\{\frac{raK_1(\beta a)K_1(\beta r)I_1(\beta r)}{K_1(\beta b)}\right\} \\ & \times F(\beta)\cos[\beta(z+\tau_2-\tau_1)]dadrd\tau_1 d\tau_2 d\beta \end{aligned} \tag{18}$$

where $m = \sqrt{j\omega\mu_z/\rho}$, λ is the mean length of the magnetic circuit in (m), μ_z is the magnetic permeability in the axial direction, ρ is the specific resistivity of the core (in Ωm), μ_1 is the permeability outside the core, N_k and N_m are the number of turns in the coils, respectively, and a and r are the middle radiuses of each coil, respectively.

Also, I_0, I_1, K_0 and K_1 are modified Bessel functions of the first and second kind, respectively, b is the mean core radius, and z is the core separation. For computation of the self-impedance of a coil with $z=0$ in (18) and $z=0.235(h+w)$ in (15), the function $F(\beta)$ is defined as,

$$F(\beta) = j\omega\mu_1\left\{\frac{f(\beta) - \frac{\mu_1}{\mu_z}f(\Gamma)}{g(\beta) + \frac{\mu_1}{\mu_z}f(\Gamma)}\right\} \tag{19}$$

where $f(x)$ and $g(x)$ are auxiliary functions, defined as

$$f(x) = x\frac{I_0(xb)}{I_1(xb)} \quad g(x) = x\frac{K_0(xb)}{K_1(xb)} \tag{20}$$

and

$$\Gamma = \sqrt{\frac{\mu_z}{\mu_r}\beta^2 + \frac{j\omega\mu_z}{\rho}} \tag{21}$$

where μ_r is the magnetic permeability in the radial direction. In practice, the ratio μ_r/μ_z is approximately 0.1. The model is verified with the measurements and computations described in [14].